Development of Numerical Prediction of Liquid Film Flows on Packing Elements in Absorbers

ISO Yoshiyuki : Doctor of Engineering, Heat & Fluid Dynamics Department, Research Laboratory, Corporate Research & Development

CHEN Xi : Ph. D, Professor, Development of Earth and Environmental Engineering, Columbia university

Gas-liquid interfacial flows, such as liquid film flows, are encountered in many industrial processes including absorption and distillation. The present study focuses on the characteristics of the transition between film flow and rivulet flow as the liquid flow rate and the wall surface texture treatments are varied. A three-dimensional gas-liquid interfacial flow simulation based on the Volume of Fluid (VOF) model has been developed. A hysteresis of the transition between the film flow and rivulet flow as the liquid flow rate changes has been discovered, which implies that the transition phenomenon depends primarily on the history of the change of the interfacial surface shape. Further study on the texture geometry shows that surface texture treatments can impede liquid channeling and increase the wetted area.

1. Introduction

Gas-liquid interfacial flows, such as liquid film flows (also known as wetting flows), are important in many industrial processes using packed columns, e.g., absorption, distillation, cooling, evaporation, and so on. Efficient control of these liquid film flows by using packing elements in packed columns is important to increase the gas-liquid interfacial area and the mass transfer rate between the gas and liquid. In general packed columns, liquid is fed from the top of the packing element and then the liquid flows down onto the packing element surface. Simultaneously, gas is fed from the bottom of the packing element and makes contact counter-currently with the liquid. There are two types of packing elements: structured packing and random packing. Structured packing elements can increase gas-liquid interfacial area efficiency and the throughput of gas flow capacity more than random packing elements. Control of liquid film flows by using packing elements is one of the key design factors in packed columns. In particular, the channeling flow of liquid significantly reduces the gas-liquid interfacial area. To prevent this phenomenon, it is very important to predict the detailed behavior of liquid film flows for the design and development of packing elements. Thus, the present study focuses on gas-liquid interfacial flows on an inclined wall, which is commonly used for structured packing elements.

There have previously been numerous theoretical and experimental studies on typical liquid film flows.[1]-[3] However, most of these studies concerned liquid film flows on smooth wall surfaces, but the effects of wall surface texture treatments on liquid film flows have not yet been clarified. Several experimental studies have been conducted for packed columns in order to measure the gas-liquid transfer rate and to develop the empirical modeling.[4]-[12] In most cases, however, the results of these studies are strongly dependent on particular device geometries and experimental conditions; few generally applicable findings have been produced.

Recently, Computational Fluid Dynamics (CFD) simulations have become a useful alternative to experiments. CFD-based prediction techniques are becoming more important because measuring liquid film flows on packing element surfaces in columns with complex geometries is very difficult and extremely expensive, especially at large industrial scales under actual flow conditions. In recent years, several studies employing CFD simulations of liquid film flows in packed columns can be found in the literature. Several useful results were obtained, including data on liquid film shape and thickness, liquid hold-up (the amount of liquid held by a packing element), gas pressure drops, and validation of CFD.[6], [9]-[17] Additionally, there are several studies of CFD-based predictions concerning not only gas-liquid two-phase film flows but also gas-liquid-liquid three-phase film flows containing two different liquids. These studies have shown that the channeling of liquid film flows is strongly influenced by three-dimensional effects.[18]-[20]

These previous efforts, which include theoretical analyses, experiments, and numerical analyses, have produced useful findings. However, detailed descriptions of the transition phenomena between the film flow and rivulet flow, as well as how such phenomena are affected by wall surface texture treatments, are still lacking. As such descriptions may contain clues for clarifying the channeling phenomenon, the present study develops a three-dimensional numerical

prediction technique using the Volume of Fluid (VOF) model and examines the effects of the change of the liquid flow rate and the wall surface texture treatments on the transition between the film flow and rivulet flow.

2. Development of the numerical prediction technique

2.1 Computational region and flow conditions

Figure 1 shows the computational region and a sample grid on a smooth inclined wall used in this study. Additionally, **Fig. 2** shows two example images of typical flow features observed on this inclined wall, namely the full film flow covering the entire inclined wall surface and the rivulet flow with liquid channeling, respectively. The gray areas in the figures indicate the wall surface in **Fig. 2**.

The geometry and flow conditions are set up according to the existing studies for liquid film flows on an inclined wall plate in order that the present simulation may be later validated by those studies.[18]-[20] As shown in **Fig. 1-(a)**, the dimensions of the inclined wall are 60 mm in the flow direction and 50 mm perpendicular to the flow direction. The wall plate is made of stainless steel and held by supports made of the same material on its left and right sides. **Figure 1** shows the computational region on a smooth surface with an inclination α of 60 degrees with respect to the horizontal ground.

Air and water are used as the gas-liquid two-phase fluids. For air, its density ρ_g is 1.185 kg/m^3 and viscosity μ_g is 1.831×10^{-5} Pa·s; for water, its density ρ_l is 997 kg/m^3, viscosity μ_l is 8.899×10^{-4} Pa·s, and surface tension σ_l is 0.072 8 N/m. The static contact angle for air and water on the wall surface θ is fixed at 70 degrees using the results from the existing experiments.[18], [19]

The inlet boundary of the liquid phase is defined by the uniform thickness of the liquid film spread evenly over the inclined plate. The main plate and both side supports are implemented as no-slip walls with the given contact angle θ (70 degrees). The other boundaries are set to the pressure outlet conditions by using the defined static pressures.
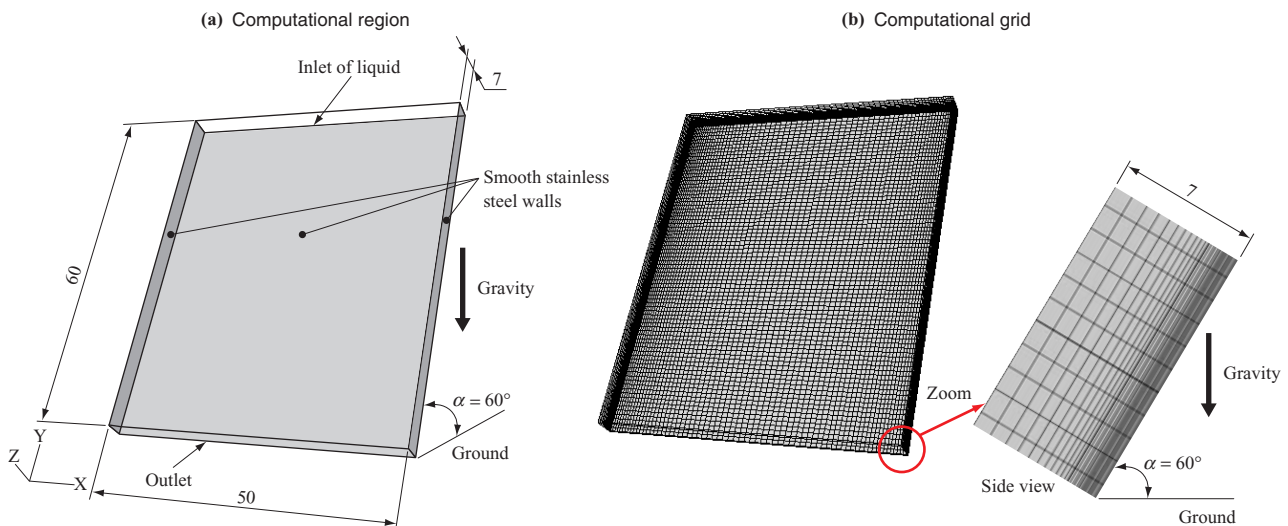
Non-uniform grids are used in the simulations such

(a) Computational region

(b) Computational grid

Fig. 1   Computational region and a sample grid for wetting flows (unit : mm)

(a) Full film flow (Full wetting flow)
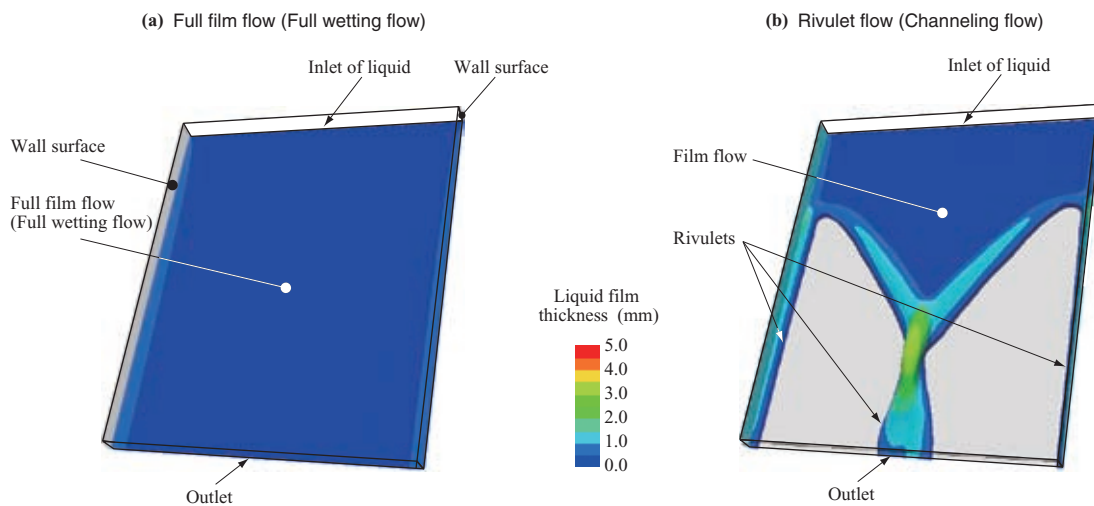
(b) Rivulet flow (Channeling flow)

Fig. 2   Two images of typical flow features in the present case (Bird's eye view)

that the grid density near the wall surface is increased in order to ensure accurate resolution for the very thin liquid flows of a thickness of several hundred micrometers. The grid density was optimized by increasing and decreasing it during several numerical tests in order to study the relationship between grid density and convergence (quasi-steady solution).

2.2 Modeling for gas-liquid interfacial flows

In this study, CFD simulations are carried out with the commercial thermal fluid flow simulation code FLUENT (Version 6.3 : ANSYS Inc.). Three-dimensional unsteady flows are simulated in the present study because existing studies have shown that the transition of gas-liquid two-phase interfacial flows cannot be simulated by using theoretical or two-dimensional numerical analyses. The Volume of Fluid (VOF) model, which is a method for tracking gas-liquid interfacial surfaces, is used to predict the behavior of gas-liquid interfacial flows with high accuracy in a reasonable computational time period.

The CFD models are based on the universal transport equations using the finite volume method. Two conservation equations of the mass and momentum are solved numerically. The mass conservation leads to the continuity equation and the momentum conservation leads to the Navier-Stokes equation as follows (The symbols used in equations (1) to (3) are described in **Table 1**.).

$$\frac{\partial \rho}{\partial t} + \nabla \cdot (\rho \cdot v) = 0 \quad \text{...} \quad (1)$$

$$\frac{\partial (\rho \cdot v)}{\partial t} + \nabla \cdot (\rho v \cdot v)$$

$$= -\nabla p + \nabla \cdot \left[\mu \left(\nabla v + \nabla v^{\mathrm{T}} \right) \right] + \rho g + S_m \quad \text{.............} \quad (2)$$

Where v and p are the velocity vector and static pressure of the fluid, respectively. S_m is the source term expressing the momentum sources such as the surface tensions, the external forces, and so on. Turbulence is not taken into account since the range of the Reynolds number of the liquid flow in this present study indicates laminar flows.

In this study, these two equations are solved by expressing the gas-liquid two-phase interfacial flows as a single fluid based on a weighted average of the physical property values of each phase in a calculation cell by the volume fraction f (Eulerian single-fluid model). To track the gas-liquid interfacial surface, it is necessary to determine the ever-changing interfacial surface position using the VOF model. The gas-liquid interfacial surface position is calculated based on the volume fraction of each phase. The transport equation of the volume fractions can be expressed in terms of convection as follows:

$$\frac{\partial (\rho_k f_k)}{\partial t} + \nabla \cdot (\rho_k f_k \cdot v_k) = S_{f_k} \quad \text{.............................} \quad (3)$$

Where f_k and v_k are the volume fraction and velocity vector of the phase k, respectively. S_f is the source term expressing the mass sources such as the mass transfer

Table 1 Nomenclature

Classification	Quantifier		Unit	Description
Symbols	v		m·s^{-1}	Velocity
	t		s	Time
	p		Pa	Static pressure
	g		m·s^{-2}	Gravitational acceleration
	S	S_m	N·m^{-3}	Source term
		S_f	kg·m^{-3}·s^{-1}	
	f		—	Volume fraction
	F		N	Force
	V		m·s^{-1}	Representative velocity
	L		m	Representative length
	Re		—	Reynolds number
	Fr		—	Froude number
	We		—	Weber number
	Q		m^3·s^{-1}	Volumetric flow rate
	w		m	Width
	A		m^2	Area
	a		m	Amplitude of the surface texture
Greek letters	α		Deg.	Inclination of the wall plate
	ρ		kg·m^{-3}	Density
	μ		Pa·s	Viscosity coefficient
	σ		N·m^{-1}	Surface tension
	θ		Deg.	Contact angle for air and water on the wall
	δ		m	Liquid film thickness
	λ		m	Length of surface texture
Subscripts	l			Liquid phase
	g			Gas phase
	m			Momentum
	k			Phase k
	f			Volume fraction
	i			Inertia
	v			Viscosity
	gr			Gravity
	st			Surface tension
	N			Nusselt theory
	w			Wetted interface
	t			Total area

between phases, supplied mass, and so on. In this case, S_f is deemed to be zero based on the assumption that the influence of mass transfer between gas and liquid on the gas-liquid interfacial surface is negligible.

In this VOF model, the volume fractions are assumed to be continuous in space and time, and the sum of the volume fractions in each calculation cell is always equal to unity.

$f_k = 0$ indicates that the calculation cell does not include the phase k. $f_k = 1$ indicates that the calculation cell is filled with the phase k. $0 < f_k < 1$ indicates that the calculation cell contains the interfacial surface between the phase k and one or more other phases.

The effect of surface tension along the interface between the gas and liquid is implemented with the Continuous Surface Force (CSF) model proposed by Brackbill et al.[21] The surface tension can be considered as a pressure jump across the interfacial surface. The addition of surface tension to the VOF model is reflected into the source term S_m in the momentum equation. The adhesive forces of the

gas-liquid interfacial surface to the wall are reflected in the calculation as the external force acting on both the gas and liquid phases by using the specified contact angle θ and the curvature of the interfacial surface in the calculation cell next to the wall.

3. Dominant forces on liquid flows

This section defines the four dominant forces of liquid flows covered in this study; the inertia force F_{li}, viscous force F_{lv}, gravitational force F_{lgr} and surface tension F_{lst}. Using the representative velocity V_l and representative length L_l for the computational region, the following three dimensionless groups can be obtained by normalizing the four dominant forces by the inertia force (The symbols used in equations (4) to (11) are described in **Table 1**.).

$$\frac{F_{lv}}{F_{li}} = \frac{\mu_l V_l L_l}{\rho_l V_l^2 L_l^2} = \frac{\mu_l}{\rho_l V_l L_l} = \frac{1}{\text{Re}_l} \quad \text{............................ (4)}$$

$$\frac{F_{lgr}}{F_{li}} = \frac{\left(\rho_l - \rho_g\right) g L_l^3}{\rho_l V_l^2 L_l^2} \approx \frac{g L_l}{V_l^2} = \frac{1}{\text{Fr}_l} \quad \text{..................... (5)}$$

$$\frac{F_{lst}}{F_{li}} = \frac{\sigma L_l}{\rho_l V_l^2 L_l^2} = \frac{\sigma}{\rho_l V_l^2 L_l} = \frac{1}{\text{We}_l} \quad \text{..................... (6)}$$

In this paper, these three dimensionless groups—the Reynolds number Re_l, Froude number Fr_l and Weber number We_l — are used as indices for considering the behavior of liquid flow.

Next, these three indices are redefined by using the Nusselt theory [1] expression for liquid film flows, which are a type of liquid flow, and substituting the representative velocity V_l and representative length L_l with specific values for liquid film velocity and thickness. Using the Nusselt theory expressions, the thickness of the liquid film flow completely developed over the whole plate area, δ_N, can be expressed as follows:

$$\delta_\text{N} = \left[\frac{3\mu_l \cdot Q_l}{\left(\rho_l - \rho_g\right) \cdot g \sin\alpha \cdot w}\right]^{\frac{1}{3}} \quad \text{............................ (7)}$$

Where Q_l is the volumetric flow rate of liquid. w is the width of the liquid film (perpendicular to the flow direction), which is assumed to be equal to the inclined plate width as the full film flow develops completely over the whole plate area. Using the velocity $V_{l\text{N}}$ and thickness δ_N of the liquid film, these three dimensionless groups can be redefined as:

$$\text{Re}_{l\text{N}} = \frac{\rho_l \cdot V_{l\text{N}} \cdot \delta_\text{N}}{\mu_l} \quad \text{................................. (8)}$$

$$\text{Fr}_{l\text{N}} = \frac{V_{l\text{N}}^2}{g \cdot \delta_\text{N}} \quad \text{................................. (9)}$$

$$\text{We}_{l\text{N}} = \frac{\rho_l \cdot V_{l\text{N}}^2 \cdot \delta_\text{N}}{\sigma} \quad \text{.......................... (10)}$$

Where $V_{l\text{N}}$ is the space-average velocity of liquid film

according to:

$$V_{l\text{N}} = \frac{Q_l}{\delta_\text{N} \cdot w} \quad \text{... (11)}$$

In particular, the Weber number $\text{We}_{l\text{N}}$, indicating the relative effects of the inertia force and surface tension, is an important parameter when evaluating the flow transition phenomenon between the film flow and rivulet flow. In the following section, these indices are used to describe the results of the present simulation.

4. Results and discussion

4.1 Transition between the film flow and rivulet flow on the smooth inclined wall

In this section, the effects of the change of liquid flow rate on the flow transition between the liquid film flow and rivulet flow on the smooth inclined plate are investigated. In **Fig. 3**, changes in the calculated wetted area ratio A_w/A_t (the ratio of the wetted area A_w to the total area of the inclined plate A_t) obtained in the present simulation are plotted against the Weber number $\text{We}_{l\text{N}}$ and compared with the existing experimental data. Changes in the flow pattern of the gas-liquid interfacial surface are visualized in **Fig. 4** for different Weber numbers (All are viewed from the direction perpendicular to the inclined wall, using the iso-surfaces which are defined by the specific volume fraction of liquid, $f_l = 0.5$. Gray areas indicate the wall surface.).

Two types of flow patterns are observed in **Fig. 4**: the full film flow, which is developed on the entire plate, and the rivulet flows caused by channeling under the present flow condition. As **Fig. 4** indicates, the decrease in the wetted area by the channeling flow at lower Weber numbers occurs. This is due to the effect of surface tension, which tends to minimize the interfacial surface area against the inertia force.

One new interesting finding in this paper is that as the Weber number increases and then decreases the transition point is quite different for the liquid film flow developing on the whole plate area (as the wetted area ratio A_w/A_t is equal to unity) from the transition point for the rivulet flow caused by channeling (as the wetted area ratio A_w/A_t gets smaller than unity).

This result indicates that the hysteresis phenomenon occurs in the transitions between the film flow and rivulet flow during the liquid flow rate (or Weber number) increases and then decreases. When the liquid flow rate increases, the wetted area increases continuously by transitioning from the rivulet flow to the film flow. When the liquid flow rate decreases, however, the wetted area decreases suddenly by discontinuous transitioning from the rivulet flow to the film flow at a lower Weber number compared with the critical Weber number when the flow rate increases. We think that the main reason for the occurrence of the hysteresis in the transition of the flow patterns is that the transition processes between the film flow and rivulet flow are different when the liquid flow rate increases or decreases, and such transitions depend strongly on the history of the liquid flow (the history
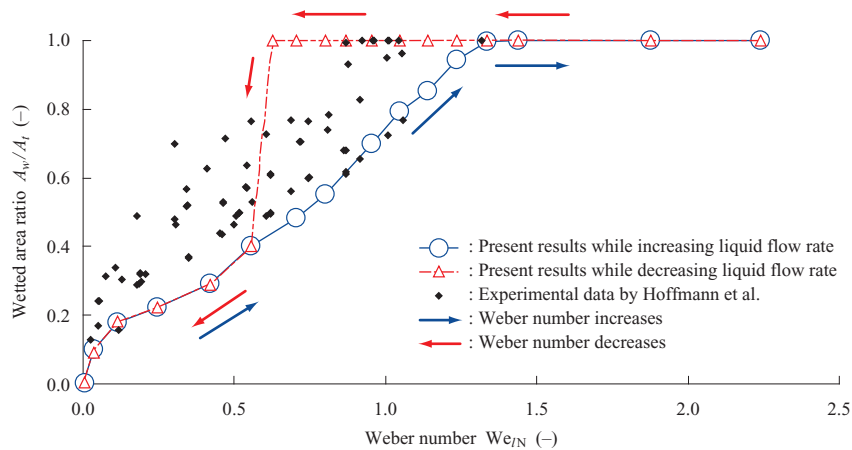
(Note) A_w : Wetted area on the inclined plate
A_t : Total area of the inclined plate

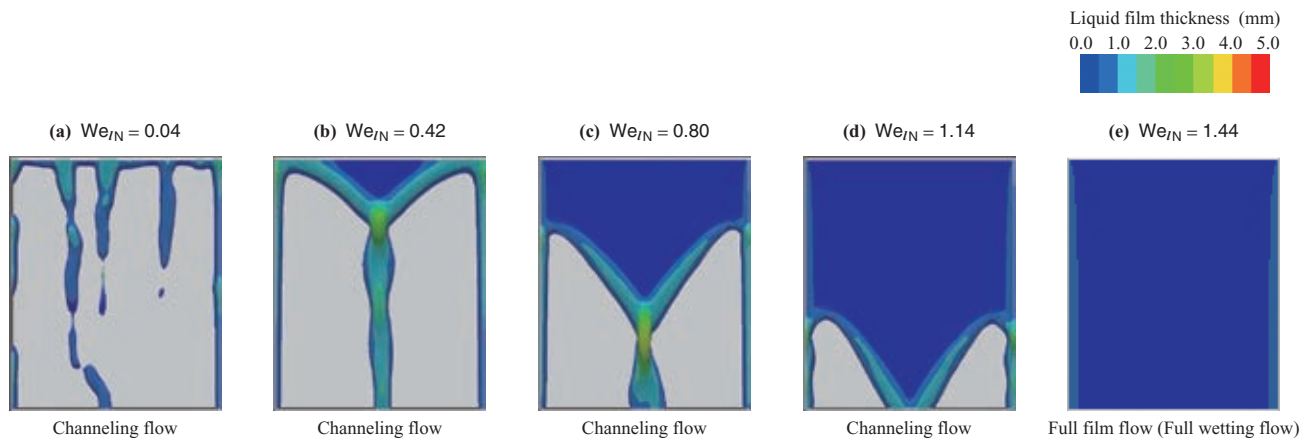Fig. 3 Wetted area ratios A_w/A_t as a function of the Weber number We_{lN}

(a) $We_{lN} = 0.04$ (b) $We_{lN} = 0.42$ (c) $We_{lN} = 0.80$ (d) $We_{lN} = 1.14$ (e) $We_{lN} = 1.44$

Channeling flow   Channeling flow   Channeling flow   Channeling flow   Full film flow (Full wetting flow)

Fig. 4 Instantaneous liquid flow patterns visualized using interfacial surfaces between gas and liquid
(Results on the smooth wall while the liquid flow rate is increasing)

of changes in interfacial surface shape).

As the liquid flow rate increases for transitioning from the rivulet flow to the film flow, the rivulet width expands gradually in the span-wise direction and the wetted area increases and then the full film flow is finally formed. Conversely, when the liquid flow rate decreases for transitioning from the liquid film flow to the rivulet flow, the thickness of the liquid film decreases gradually and then the rivulet flow is suddenly formed when a breakup occurs due to a crack in a part of the liquid film. Therefore, the transition processes between the film flow and rivulet flow are different when the liquid flow rate increases or decreases, and also the energy barriers needed for these two transition processes differ in the directions of flow pattern transition. This is why the hysteresis occurs. Though the disturbance (flow fluctuation in space and time) and the hysteresis of the contact angle (advancing, receding and dynamic changes) may occur under actual conditions, they are not considered in the present simulation. These may result in more complicated phenomena in the transition processes.

The range within which the liquid flow transition between the film flow and rivulet flow occurs predicted by the present simulation of the increasing and decreasing of Weber numbers matches reasonably with the experimental results in Fig. 3, which has validated the present approach.

Additionally, the simulated flow behavior on the interfacial surface shown in Fig. 4 also agrees well with the existing experimental data [19] at several points, such as the position of liquid film breakup and rivulet width. These validations demonstrate that the present simulation, which uses this VOF model, is capable of predicting gas-liquid interfacial flow on an inclined smooth wall with high accuracy in a reasonable calculation time period (approx. several days per case).

4.2 Effects of wall surface texture treatments on gas-liquid interfacial flow

Wall surface treatments, such as intended small textures or perforations, are often used in the several commercial industrial packing elements in order to prevent liquid channeling and to promote mixing of flow in the liquid film.[9], [10], [12]-[14] In this section, the effects of wall surface

texture treatments on the gas-liquid interfacial flow are investigated.

Figure 5 is a schematic that shows the outline and geometry of the wavy surface texture on the inclined wall used in the present simulation. The amplitude a and length λ of the wavy surface texture are selected based on a commercially available industrial packing element.[(12), (14)] In this case, the amplitude of the wavy surface texture is of the same order as the thickness of the liquid film formed on the wall surface.

Figure 6 shows the calculated wetted area ratio A_w/A_t obtained by the present simulation as a function of the Weber number We_{lN}. It is quantitatively made clear how appropriate wall surface texture treatments will be useful to give a larger wetted area under the same flow condition.

The simulation results of the changes in flow behavior on the gas-liquid interfacial surface for different Weber numbers are visualized in **Fig. 7** (All are viewed from the direction perpendicular to the inclined wall, using the iso-surfaces which are defined by the specific volume fraction of liquid, $f_l = 0.5$. Gray areas indicate the wall surface.). The effects of the wall surface texture treatment on the liquid flow behavior can be seen by comparing the simulated liquid flow patterns on the wall surface texture in **Fig. 7** with those on the smooth wall in **Fig. 4** at the same condition of Weber number. For example, the channeling flow occurs in the case of the smooth wall at $We_{lN} = 1.14$ in **Fig. 4**, yet at the same Weber number condition the full film flow is retained on the full plate with the assistance of the texture treatment in **Fig. 7**. Thus, the present results show that the surface texture treatments can indeed help to prevent liquid channeling and can increase the wetted area.
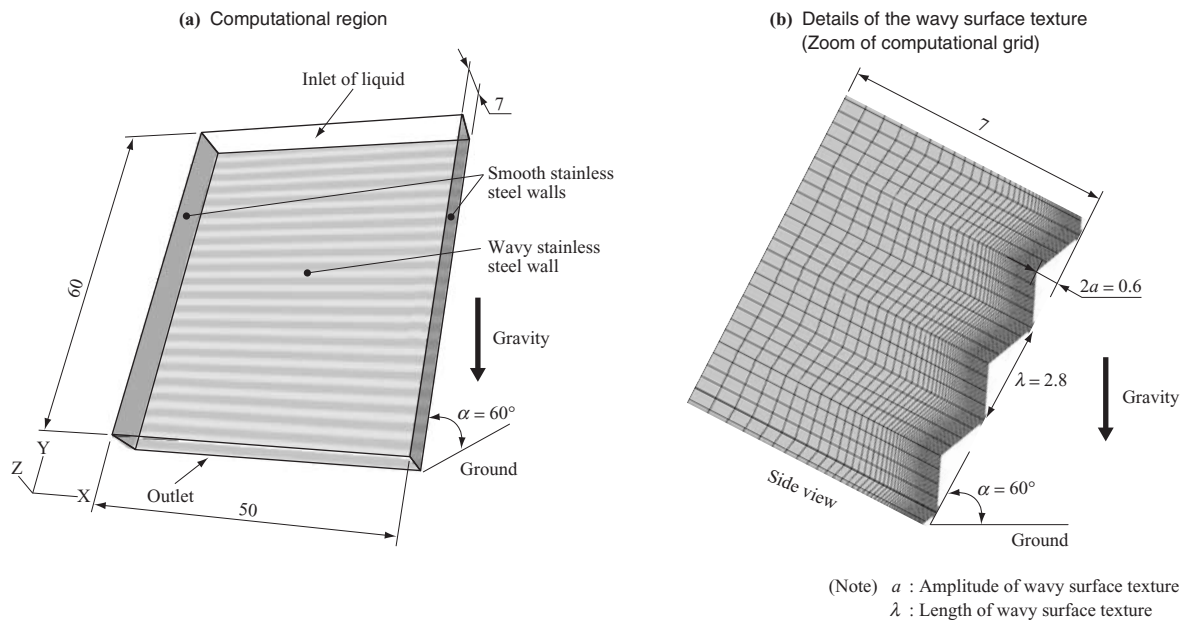

(a) Computational region

(b) Details of the wavy surface texture
(Zoom of computational grid)

(Note) a : Amplitude of wavy surface texture
λ : Length of wavy surface texture

Fig. 5　Computational region and a sample grid for wetting flows with wall surface texture treatments (unit : mm)

(Note) A_w : Wetted area on the inclined plate
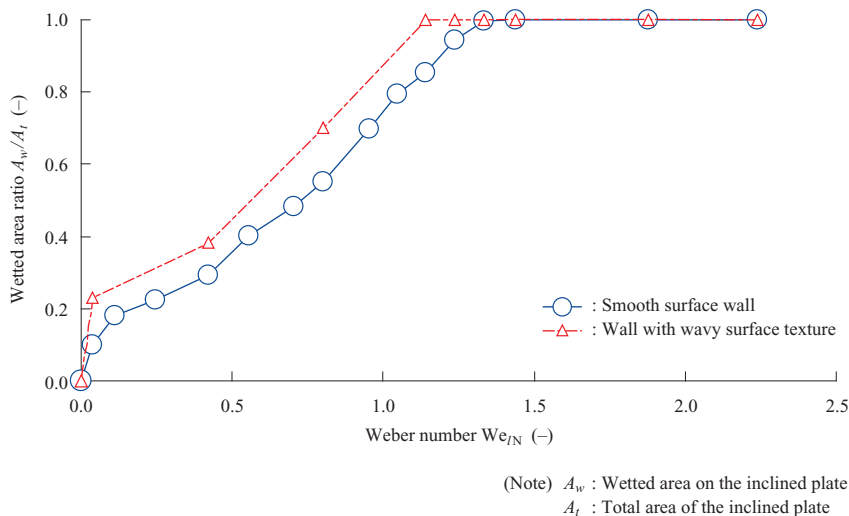A_t : Total area of the inclined plate

Fig. 6　Wetted area ratios A_w/A_t as a function of the Weber number We_{lN} (While the liquid flow rate is increasing)
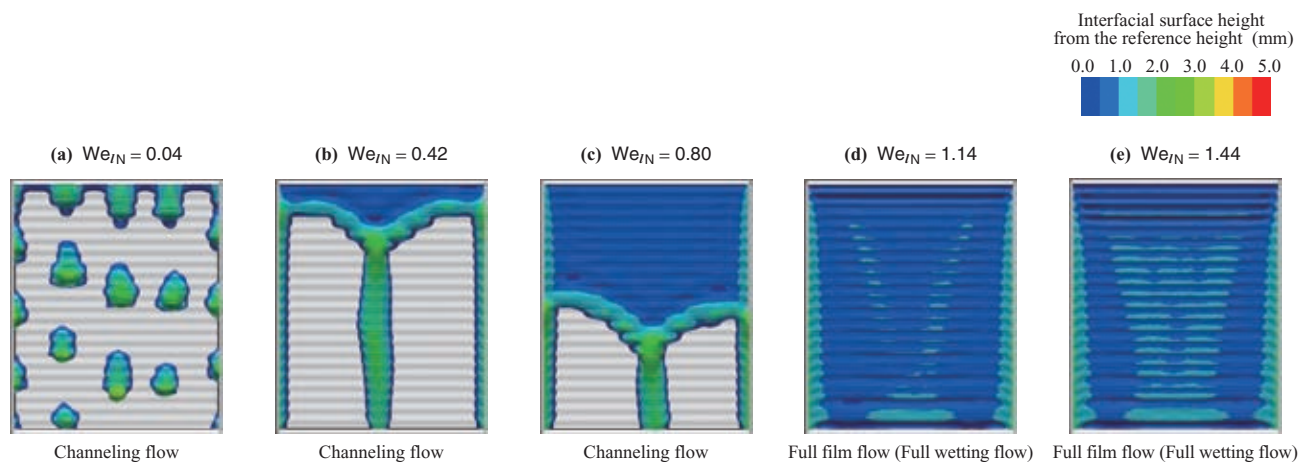
Fig. 7 Instantaneous liquid flow patterns visualized using interfacial surfaces between gas and liquid
(Results of simulation of the wall surface texture treatment while the liquid flow rate is increasing)

5. Conclusion

In packed columns, channeling of liquid film flow causes significant reductions in gas-liquid interfacial area. This study focuses on the transition phenomenon between the film flow and rivulet flow on inclined walls commonly used for structured packing elements, the effects of which were investigated by using the three-dimensional simulation we developed with the VOF model. Our new findings include the following.

(1) An interesting hysteresis phenomenon in the flow transition between the film flow and rivulet flow on the inclined plate was discovered during the liquid flow rate (or Weber number) increases and then decreases. We think that the main reason for the occurrence of the hysteresis in the transition of the flow patterns is that the transition processes between the film flow and rivulet flow are different when the liquid flow rate increases or decreases, and such transitions depend strongly on the history of the liquid flow (the history of changes in interfacial surface shape). This finding about the transition phenomenon of flow patterns can be applied to other studies to grasp the details of transition processes as well as to facilitate the control of liquid flow rates and the development of packing elements for assuring the efficient gas-liquid interfacial area.

(2) The simulation results agree well with the existing experimental data at points such as the critical Weber number that causes the transition between the film flow and rivulet flow as well as the gas-liquid interfacial surface shape. These validations demonstrate that the present simulation, which uses the VOF model, is capable of predicting gas-liquid interfacial flow on a smooth inclined plate with a high accuracy in a reasonable calculation time period.

(3) The present simulations show quantitatively that surface texture treatments can help to prevent liquid channeling and can increase the wetted area through the comparison of two geometry cases (with and without the surface texture).

Using this prediction technique, we will carry out further systematic investigations of the effects of packing elements' wall surface texture treatments on the gas-liquid interfacial flow, and we will apply our results to the development of packing elements that can improve the performance of packed columns. We will also carry out numerical prediction under the flow conditions used in various industrial processes as well as for packing elements with more complicated geometries in order to further advance this technique for design and development of entire columns.

REFERENCES

(1) W. Nusselt : Die oberflachenkondensation des wasserdampfes   Zeitschr. Ver. Deut. Ing. 60 (1916) pp. 541-546 and pp. 569-575

(2) L. Phan and A. Narain : Nonlinear stability of the classical Nusselt problem of film condensation and wave effects   Transaction of the ASME Journal of Applied Mechanics Vol. 74 (2007. 3)   pp. 279-290

(3) X. Wang, M. He , H. Fan and Y. Zhang : Measurement of falling film thickness around a horizontal tube using laser-induced fluorescence technique   Journal of Physics Conference Series 147 (2009)   012039

(4) J. L. Bravo, J. A.Rocha and J. R. Fair : Mass transfer in gauze packings   Hydrocarbon Processing 64 (1985)   pp. 91-95

(5) J. L. Bravo, J. A.Rocha and J. R. Fair : A comprehensive model for the performance of columns containing structured packings   Inst. Chem. Eng. Symp. Series 128 (1992)   pp. A439-A457

(6) L. Spiegel and W. Meier : Distillation columns with structured packings in the next decade Trans. IChemE Vol. 81 Issue1 Part A (2003. 1) pp. 39-47

(7) C. R. Murrieta, A. F. Seibert, J. R. Fair and J. A. Rocha-U : Liquid-side mass-transfer resistance of structured packings Ind. Eng. Chem. Res. 43 (22) (2004. 9) pp. 7 113-7 120

(8) R. Sidi-Boumedine and L. Raynal : Influence of the viscosity on the liquid hold-up in trickle-bed reactors with structured packings Catalysis Today Vol. 105 Issue 3-4 (2005. 8) pp. 673-679

(9) A. Ataki, P. Kolb, U. Buhlman and H. J. Bart : Wetting performance and pressure drop of structured packings : CFD and experiment IChemE Symposium Series 152 (2006) pp. 534-543

(10) A. Ataki and H. J. Bart : Experimental and CFD simulation study for the wetting of structured packing element with liquid Chemical Eng. and Tech. Vol. 29 Issue 3 (2006. 3) pp. 336-347

(11) J. Chen, C. Liu, Y. Li, Y. Huang, X. Yuan and G. Yu : Experimental investigation of single-phase flow in structured packing by LDV Chin. J. Chem. Eng. Vol. 15 Issue 6 (2007. 12) pp. 821-827

(12) L. Raynal, F. B. Rayana and A. Royon-Lebeaud : Use of CFD for CO_2 absorbers optimum design : from local scale to large industrial scale Energy Procedia Vol. 1 Issue 1 (2009. 2) pp. 917-924

(13) P. Valluri, O. K. Matar, G. F. Hewitt and M. A. Mendes : Thin film flow over structured packings at moderate Reynolds numbers Chemical Eng. Science Vol. 60 Issue 7 (2005. 4) pp. 1 965-1 975

(14) L. Raynal and A. Royon-Lebeaud : A multi-scale approach for CFD calculations of gas-liquid flow within large size column equipped with structured packing Chemical Eng. Science Vol. 62 Issue 24 (2007) pp. 7 196-7 204

(15) E. Y. Kenig : Complementary modeling of fluid separation processes Chemical Engineering Research and Design Vol. 86 Issue 9 (2008. 9) pp. 1 059-1 072

(16) W. Ludwig and J. Dziak : CFD modelling of a laminar film flow Chemical and Process Eng. 30 (2009) pp. 417-430

(17) H. Lan, J. L. Wegener, B. F. Armaly and J. A. Drallmeier : Developing laminar gravity-driven thin liquid film flow down an inclined plane Trans. ASME J. Fluids Engineering Vol. 132 Issue 8 081301 (2010. 8) pp. 1-8

(18) A. Hoffmann, I. Ausner, J. U. Repke and G. Wozny : Fluid dynamics in multiphase distillation processes in packed towers Computers and Chemical Eng. Vol. 29 Issue 6 (2005. 5) pp. 1 433-1 437

(19) A. Hoffmann, I. Ausner, J. U. Repke and G. Wozny : Detailed investigation of multiphase flow behaviour on inclined plates Trans. IChemE, Chemical Eng. Research and Design Vol. 84 Issue 2 (2006) pp. 147-154

(20) J. U. Repke, I. Ausner, S. Paschke, A. Hoffmann and G. Wozny : On the track to understanding three phases in one tower Trans. IChemE, Chemical Eng. Research and Design Vol. 85 Issue 1 (2007) pp. 50-58

(21) J. U. Brackbill, D. B. Kothe and C. Zemach : A continuum method for modeling surface tension J. of Comp. Physics Vol. 100 No. 2 (1992. 6) pp. 335-354